A unique multidrug nanomedicine made of squalenoyl-gemcitabine and alkyl-lysophospholipid edelfosine

C Rodríguez-Nogales, V Sebastián, S Irusta, D Desmaële, P Couvreur, M J Blanco-Prieto

A unique multidrug nanomedicine made of squalenoyl-gemcitabine and alkyl-lysophospholipid edelfosine

C. Rodríguez-Nogales[a,b], V. Sebastián[c,d], S. Irusta[c,d], D. Desmaële[e], P. Couvreur[e*], M.J. Blanco-Prieto[a,b*]

[a] *Pharmacy and Pharmaceutical Technology Department, University of Navarra, Pamplona, Spain*

[b] *Instituto de Investigación Sanitaria de Navarra (IdiSNA), Pamplona, Spain*

[c] *Department of Chemical and Environmental Engineering & Institute of Nanoscience of Aragon (INA), University of Zaragoza, Zaragoza, Spain*

[d] *Networking Research Center on Bioengineering, Biomaterials and Nanomedicine, CIBER-BBN, 28029-Madrid, Spain.*

[e] *Institut Galien Paris-Sud, UMR CNRS 8612, Université Paris-Sud, Université Paris-Saclay, Châtenay-Malabry Cedex, France*

*Correspondence to: M.J. Blanco-Prieto, Department of Pharmacy and Pharmaceutical Technology, School of Pharmacy, University of Navarra, C/Irunlarrea 1, 31080 Pamplona, Spain. Tel: +34 948425679, Fax: 34 948425740. E-mail: mjblanco@unav.es – Prof Patrick Couvreur, Université Paris-Sud, Institut Galien, UMR CNRS 8612 – France. Te: +33 1 46835396, Fax: 34 948425740. E-mail: patrick.couvreur@u-psud.fr

ABSTRACT

Among anticancer nanomedicines, squalenoyl nanocomposites have obtained encouraging outcomes in a great variety of tumors. The prodrug squalenoyl-gemcitabine has been chosen in this study to construct a novel multidrug nanosystem in combination with edelfosine, an alkyl-lysophopholipid with proven anticancer activity. Given their amphiphilic nature, it was hypothesized that both anticancer compounds, with complementary molecular targets, could lead to the formation of a new multitherapy nanomedicine. Nanoassemblies were formulated by the nanoprecipitation method and characterized by dynamic light scattering, transmission electron microscopy and X-ray photoelectron spectroscopy. Because free edelfosine is highly hemolytic, hemolysis experiments were performed using human blood erythrocytes and nanoassemblies efficacy was evaluated in a patient-derived metastatic pediatric osteosarcoma cell line. It was observed that these molecules spontaneously self-assembled as stable and monodisperse nanoassemblies of 51 •± 1 nm in a surfactant/polymer free-aqueous suspension. Compared to squalenoyl-gemcitabine nanoassemblies, the combination of squalenoyl-gemcitabine with edelfosine resulted in smaller particle size and a new supramolecular conformation, with higher stability and drug content, and ameliorated antitumor profile.

KEYWORDS

Cancer, chemotherapy, multidrug nanomedicine, nanoassemblies, squalene, gemcitabine, edelfosine, pediatric osteosarcoma

1. INTRODUCTION

The current limitations of conventional chemotherapy have prompted the implementation of nanomedicine to improve cancer treatment. Interest is now focusing on nanocarriers to administer antitumor agents and exploit their intrinsic potential for providing more effective and safer treatments.[1] These nanosized suspensions are able to improve the therapeutic index of encapsulated drugs by modifying drug pharmacokinetics and tissue distribution.[2-4]. Nonetheless, it is disappointing to note that as the search for novel nanotechnology approaches to cancer treatment intensifies, most of these nanotherapies are failing to reach the clinic stages. We may anticipate that some of the reasons for this failure are linked to drug burst release behavior together with low drug entrapment rates. These and other limitations are sometimes detrimental when it comes to achieving a correct therapeutic window and can even trigger toxicities in cancer patients.[5] Until these issues are resolved, nanotechnology approaches will be unlikely to offer therapeutic progress in comparison to free drug administration.

In order to address these limitations, a new technology based on the “squalenoylation” concept has been developed. The bioconjugation of drugs to squalenic acid (SQ-COOH), a nontoxic and biocompatible lipid squalene-derived molecule, leads to the formation of squalenoyl prodrugs able to self-assemble in supramolecular structures to form stable nanocomposites.[6-9] In this way, each cytostatic drug molecule is chemically linked to its SQ-COOH counterpart, which ensures a high drug loading. As it is a prodrug, drug burst release from the NPs is avoided. An additional advantage is that neither polymers nor surfactants are needed to form the NPs. Among the squalenoyl nanoassemblies (NAs) investigated, considerable activity has centered on squalenoyl-gemcitabine (SQ-gem) NAs.[10-12]. Gemcitabine (Gem) is a nucleoside analogue that is very active against various tumors, incl. pancreatic cancer, non-small-cell lung cancer and ovarian cancer.[13,14] Its antitumor efficacy is, however, restrained due to rapid

extra- and intracellular deamination, as well, as to resistances mainly associated with nucleoside transporter HENT1 downregulation.[15] Thus, SQ-gem NAs have shown an improved anti-cancer activity compared to free Gem in murine tumor models of pancreas or leukemia. Such higher therapeutic index was attributed to reduced drug metabolization, resulting in higher blood concentration, better biodistribution and increased intracellular penetration which is independent of the HENT1 transporter.[16,17].

In order to further improve the above-mentioned nanoformulation we took into consideration some aspects. On the one hand, cancer treatment is often inefficient when using a single anticancer drug and several multitherapy approaches have been proposed [18]. We suggest that the co-encapsulation of another drug with a distinct therapeutic target may enhance the anticancer potential of the SQ-gem NAs. On the other hand, since squalenoyl prodrugs display an amphiphilic structure that allows them to self-assemble into nanocomposites, it was hypothesized that to achieve a successful multidrug approach, the additional drug should possess an amphiphilic character too.[19]

We selected the amphiphilic drug edelfosine (EF), an alkyl-lysophospholipid with proven anticancer activity in several tumors [20–22]. Unlike Gem, exerting anticancer activity through DNA synthesis inhibition, EF acts on a completely different pharmacological target. Although the exact cell death mechanisms are not fully elucidated, EF is reported to selectively accumulate in tumor cell membranes, inducing Fas receptor clustering and activation on lipid rafts, triggering cellular apoptosis [23–24]. Moreover, we have previously demonstrated that the nanoencapsulation of EF considerably augmented the therapeutic index in comparison with its free counterpart when administered *in vivo* [25,26]. Here, we investigate whether the physical mixture of these two compounds (*i.e.* SQ-gem and EF) could lead to the formation of a functional multidrug nanomedicine (Fig. 1A). The hydrodynamic properties of this nanoformulation were analyzed by dynamic light scattering (DLS) and cryo-Transmission electron microscopy (TEM). In order to elucidate the new structure and composition of the new coassembly, TEM UHPLC/MS/MS and X-ray photoelectron spectroscopy (XPS) analyses were performed. The hemolysis activity of encapsulated EF was analyzed using human blood erythrocytes and the anticancer activity was tested in patient-derived metastatic pediatric osteosarcoma cells.

Here, we investigate whether the physical mixture of these two compounds (ie. SQ-gem and EF) could lead to the formation of a functional multitherapy nanomedicine (Figure 1). We characterized the hydrodynamic properties, morphology, macromolecular organization and stability of this novel nanoformulation whose anticancer efficacy has been tested *in vitro* in pediatric osteosarcoma cells.

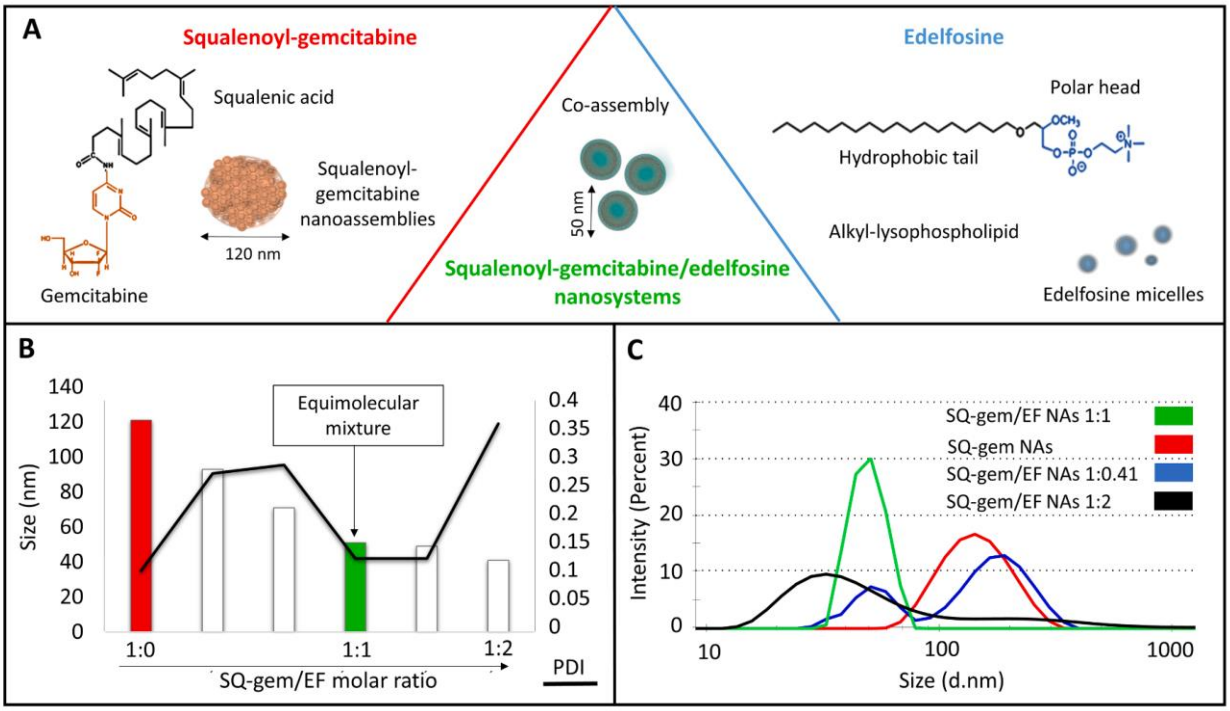

Fig. 1. (A) Diagram of the formation of the new NAs. The physical mixture of SQ-gem and EF leads to the formation of SQ-gem/EF NAs. (B) Effect of the SQ-gem:EF molar ratio on the particle size and PDI. (C) Size distribution by intensity peaks corresponding to SQ-gem/EF NAs (green), SQ-gem NAs (red) and to a mixture of SQgem and EF at a molar ratio 1:0.41 (blue), and 1:2 (black). (For interpretation of the references to colour in this figure legend, the reader is referred to the web version of this article.)

2. Materials and methods

2.1. Materials

Gemcitabine hydrochloride was purchased from Carbosynth, Ltd. (Compton, UK). Edelfosine was obtained from Apointech (Salamanca, Spain). The synthesis of squalenoyl acid and squalenoyl-gemcitabine and 1,10,2-tris-nor-squalenic acid was performed as previously described[9] (see SI for further information). Ethanol absolute was purchased from Panreac Química (Barcelona, Spain). Phosphotungstic acid hydrate was purchased from Sigma Aldrich (Barcelona, Spain). Amicon Ultra-15 10 kD MWCO filter devices were provided by Millipore (Cork, Ireland) and all reagents employed for mass spectroscopy (gradient grade for liquid chromatography) were obtained from Merck (Barcelona, Spain). Celltiter 96® aqueous one solution cell proliferation assay (MTS) was purchased from Promega (Alcobendas, Spain). Heat inactivated fetal bovine serum, Trypsin-EDTA and penicillin/streptomycin were provided by Gibco® (Invitrogen Inc., Carlsbad, USA). Phosphate Buffer Saline (PBS) and McCoy's 5A cell medium were purchased from Lonza (Verviers, Belgium). Tissue cell culture 96-well plate was provided by Corning Inc. (New York, USA).

2.2. Preparation of nanocomposites

Squalenoyl nanocomposites were prepared using the nanoprecipitation method. Briefly, a solution of SQ-gem in ethanol (200 μL at 11.6 μmol mL^{-1}) alone or mixed with a

solution of EF (200 μL at 11.6 μmol mL^{-1}) was added dropwise under stirring (500 rpm) into 2 mL of distilled water. Nanoprecipitation of the SQ-gem NAs or SQ-gem/EF NAs occurred spontaneously. Ethanol was completely evaporated in a vacuum using a Rotavapor (Buchi R-210/215, Buchi Corp., Canada) to obtain an aqueous suspension of SQ-gem NAs or SQ-gem/EF NAs. SQCOOH NAs (200 μL at 18.75 μmol mL^{-1}) and SQCOOH NAs loaded with EF (SQCOOH/EF NAs) at a SQCOOH: EF molar ratio of 2:1 (200 μL at 9.375 μmol mL^{-1} of EF), were prepared employing the same procedure as described above for SQ-gem NAs and SQ-gem/EF NAs.

Mean particle size and polydispersity index (PDI) of the NAs were determined at 25ºC by dynamic light scattering (Zetasizer Nano ZS Malvern; Malvern Instruments SA, UK) after 1:15 dilution in ultrapure water. Surface charge of the NPs was characterized by measuring the zeta potential with laser Doppler velocimetry (Zetasizer Nano ZS Malvern; Malvern Instruments SA, UK). Drug recoveries from the NAs were quantified with Ultra-high performance liquid chromatography-tandem mass spectrometer (UHPLC–MS/MS) after washing the formulations with Amicon Ultra-15 10 kD MWCO filter devices (3x10 mins, 4ºC, 5.000 r.p.m).

2.3. UHPLC–MS/MS method

An UHPLC/MS/MS method based on modifications of Estella-Hermoso de Mendoza *et al.* for EF[27] and of Khoury *et al.* for SQ-gem[28] was optimized to perform the simultaneous determination of SQ-gem and EF. The UHPLC system was composed of an Acquity UPLC™ system (Waters Corp., Milford, MA, USA). Separation was carried out on an Acquity UPLC™ BEH C_{18} column (50mm×2.1mm, 1.7m; Waters Corp., Milford, MA, USA) with a gradient elution, using a mobile phase starting from 30% of a 1% formic acid aqueous solution and 70% of methanol.

Triple-quadrupole tandem mass spectrometric detection was performed on an Acquity™ TQD mass spectrometer (Waters Corp., Milford, MA, USA) with an electrospray ionization (ESI) interface. The mass spectrometer operated in positive mode was set up for multiple reaction monitoring (MRM) to monitor the transition of m/z 524.3→104.2 for EF and the transition of m/z 646.7→112 for the SQ-gem. Data acquisition and analysis were performed using the MassLynx™ (for further details see SI).

2.4. Electron microscopy imaging

The morphology of squalenoyl nanocomposites was characterized by Transmission electron microscopy (TEM), using negative staining, or by cryo-Transmission electron microscopy (cryo-TEM), using cryogenic freezing. Electron microscopy images were recorded on a T20-FEI Tecnai thermoionic microscope operated at an acceleration voltage of 200 kV. Aberration corrected scanning transmission electron microscopy (Cs-corrected STEM) images were acquired using a high angle annular dark field detector (HAADF) in a FEI XFEG TITAN electron microscope operated at 300 kV and equipped with a CETCOR Cs-probe corrector from CEOS. Fast Fourier Transform (FFT) analysis was used to shed light on the internal structure and assembly of the NPs.

Negative stained samples were prepared by dropping 20 µl of sample in carbon coated copper grids (200 mesh), dried at room temperature and stained with a negative staining agent (phosphotungstic acid). The grid preparation of cryogenically immobilized samples required an extremely rapid sample freezing to achieve a vitreous state. A thin film vitrified specimen was prepared with a Vitrobot (FEI) in melting ethane. Afterwards, the sample holder with the specimen grid was maintained under cryogenic conditions with liquid nitrogen.

2.5. XPS assays

X-ray photoelectron analysis (XPS) was performed with an AXIS Supra (Kratos Tech.). The spectra were excited by a monochromatic AlK source (1486.6 e.V) run at 15 kV and 15 mA. The photoelectron takeoff angle (angle of the surface with the direction in which the photoelectrons are analyzed) was 90°. For the individual peak regions, a pass energy of 20 eV was used. Peaks were analyzed with the CasaXPS software. Atomic concentration of each element was calculated by integration of each element main peak, taking into account the corresponding atomic sensitivity factors (ASF). The composition of the material was analyzed at different depths after sputtering the surface of the sample for a certain time using a gas cluster ion source. Argon ion clusters of mean size 1000 atoms and energy 10kV were used for etching.

2.6. Hemolysis evaluation

Erythrocytes were separated from human blood plasma by centrifugation (4000xg, for 7 min), washed with PBS 3-times and diluted with 50 ml of PBS. Then, 0.5 ml of this suspension was added to 1.5 mL of free and nanoformulations of EF. Incubation with PBS served as negative control and with Triton X-100 as positive control. After 1 h, the samples were centrifuged (4000 xg, for 7 min) and the supernatants absorbance was measured in an Agilent 8453 UV-visible spectrophotometer (Agilent, CA, USA) at 540 nm.

2.7. Cell culture

The cell line used throughout the study was the human immortalized osteosarcoma cell line U-2 OS (ATCC® HTB96™), purchased from the American Type Culture Collection (Sigma Aldrich). U-2 OS cell line was maintained in McCoy's 5A medium, supplemented with 10% of fetal bovine serum and 1% penicillin/ streptomycin in an incubator at 37ºC and a humidified atmosphere with 5% carbon dioxide. For the *in vitro* cytotoxicity assays U-2 OS cells were plated on 96-well plates at a density of 1.700 cells per well, 24 h before the addition of different concentrations of free and nanoparticulate Gem and EF in triplicate wells. After 72 h of incubation with the drugs the medium was withdrawn and 100 µL of complete medium containing 15 % v/v of MTS was added to each well. Absorbance was measured 3 h later in a microplate reader (iEMS reader MF, Labsystem, Helsinki, Finland) at a test wavelength of 492 nm with the reference wavelength set at 690 nm. The concentration of drug required to inhibit cell growth by 50% (IC50) was estimated by fitting the dose response curve to a sigmoidal function using the GraphPad Prism version 5.0 for Windows (GraphPad

Software, San Diego, CA, USA). Drug interaction studies were estimated based on the calculation of the combination index (CI) of the drugs at a constant ratio.

3. RESULTS AND DISCUSSION

3.1. Design and characterization of supramolecular squalene based nanoassemblies.

SQ-gem/EF nanocomposites were prepared by nanoprecipitation from an ethanolic solution as described in the Materials and Methods. By modifying the ratio of SQ-gem and EF in the squalene-based nanocomposites, it was possible to select the best nanoformulation in terms of size distribution. As seen in Fig. 1B and 1C, although initial concentrations of EF led to undesirable PDI values, concentrations the particle population homogeneity was again recovered at equimolecular. Interestingly, the mean particle size was considerably decreased from 121 ±14 nm for SQ-gem NAS to 50 ±1 nm for SQ-gem/EF NAs. However, when EF concentrations surpassed equimolarity, the mean particle size barely changed, whereas the uniformity of the particle population rapidly worsened as it was observed at the ratio SQ-Gem/EF 1:2. Of note, SQCOOH NAs and SQCOOH NAs loaded with EF were also prepared in similar conditions. As observed for SQ-gem/EF NAs, a very similar particle size reduction was noticed from 99 •± 5 nm for SQCOOH NAs to 47 •± 2 nm for SQCOOH/EF NAs. Finally, based on DLS data showing that the equimolecular mixture of both components (*ie.* SQgem and EF) led to optimal colloid properties, it was suggested that EF completely co-assembled with SQ-gem. To verify this, NAs were washed using a method previously described to efficiently separate unloaded EF from lipid NPs [20–22] and afterwards quantified by UHPLC/MS/MS. Results showed EF recoveries close to 100%, confirming the complete encapsulation/insertion of EF into SQ-gem. Unlike EF, SQ-gem is completely insoluble in aqueous medium, and therefore there is also no loss of product during the formulation process.

With respect to the changes in the particle surface charge, the results show that the incorporation of EF in the NAs brought about a slight increase in the zeta potential values (Table 1). SQ-gem NAs displayed zeta potentials of −17.73 •} 1.26 mV which was in agreement with previous studies [6,29]. On the other hand, designed and optimized SQ-gem/EF NAs (*ie.*, at a SQ-gem:EF ratio of 1:1) showed a zeta potential value of −12.56 •} 1.15 mV. Of note, EF polar head presents a negatively charged phosphate group but also a positively charged quaternary amine group, making the ionic balance neutral [30]. As Table 1 shows, independent preparations (n≥5) of the NAs demonstrated this nanoformulation as highly reproducible, giving nearly identical results for each sample. Moreover, as confirmed by UHPLC/MS/MS, this approach allowed to obtain NAs with very high overall drugs content of 67.28 wt%, containing both Gem (22.49 wt%) and EF (44.73 wt%). This is a significant improvement in terms of drug loading in comparison with common drug delivery systems, which often display much lower drug loading capacity. Such is the case with previously reported lipid nanoformulations loaded with Gem [31] or EF [25] accounting for a drug loading of 7.3 and 2.26 wt% respectively. The high drug payload of SQ-gem/EF NAs may thus help to attain a correct therapeutic window and to avoid infra/overdosing that might

provoke toxicities [3]. And given that the SQ-gem/EF NAs were built with only drugs or prodrugs, possible adverse effects derived from the incorporation of polymers, surfactants or other colloidal stabilizers may be avoided [32,33]. All the preparations were further characterized by cryo-TEM analysis. The different nanoformulations displayed spherical shape and suitable colloid characteristics, in good agreement with DLS data (Fig. 2). Again, SQ-gem/EF NAs (Fig. 2B) show a substantial particle diameter reduction compared to SQ-gem NAs (Fig. 2A). The particle size reduction towards *ca.* 50 nm resulted from the insertion of EF into SQ-gem NAs, suggesting that the amphiphilic nature of EF allowed the co-assembly with SQ-gem by means of molecular interactions between the two molecules. Importantly, such particle size reduction could improve NPs biodistribution. For instance, particles under 10 nm werereported to be rapidly filtered by the kidneys, whereas particles larger than 100 nm undergo an enhanced liver uptake [34,35]. Cabral et al. postulated that although the NP size may not affect the particle tumor distribution in hyperpermeable tumors, only NPs smaller than 70 nm, which is the case of SQ-gem/EF NAs, were able to accumulate efficiently in poorly permeable tumors such as human pancreatic adenocarcinoma [36]. Bearing in mind that Gem is given in chemotherapy for pancreatic cancer, the use of specifically designed SQ-gem/EF NAs of around 50 nm might improve the pharmacological efficacy in this type of poorly permeable tumor, by means of the so called Enhanced Permeability and Retention (EPR) effect. In any case, the EPR effect in solid tumors is not as well understood as initially thought [37] and further experiments *in vivo* are mandatory to elucidate the real behavior of SQgem/ EF NAs.

Table 1. Colloidal characteristics of squalene-based nanocomposites

	size (nm)[1]	PDI[1]	ζ (mv)[2]	% Gem[3]	% EF[3]	% total[3]
SQ-gem	121 ± 14	0.1 ± 0.02	-17.73 ±1.26	40.7	0	40.7
SQ-gem/EF	51 ± 1	0.12 ± 0.03	-12.56 ± 1.15	22.49	44.73	67.28
SQCOOH	99 ± 5	0.12 ± 0.01	-29.8 ± 2.91	0	0	0
SQCOOH/EF	47 ± 2	0.267 ± 0.03	-23.76 ± 5.17	0	39.57	39.57

[1]Determined by DLS. [2]Zeta potential. [3]% = MWdrug/MWnanocomposites.

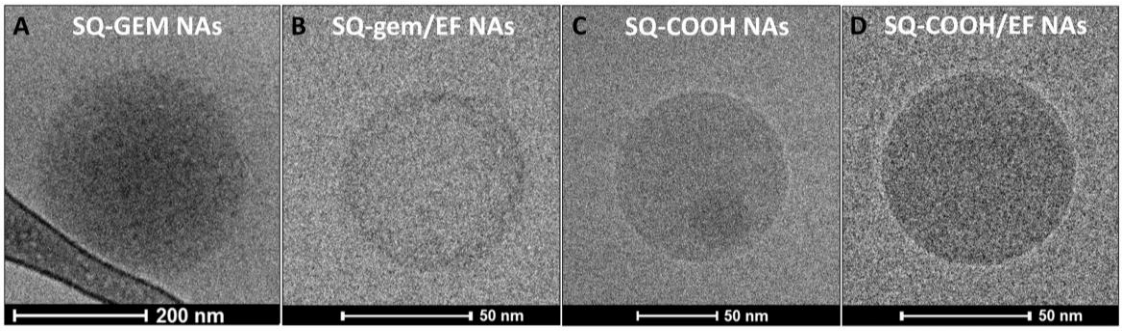

Fig.2. Morphological characterization of squalene-based nanocomposites. Cryogenic transmission electron microscopy of SQ-gem (A), SQ-gem/EF (B), SQ-COOH (c) and SQ-COOH/EF nanocomposites.

3.2. Macromolecular conformation

Negatively stained TEM analysis also revealed striking morphological differences between SQ-gem and SQ-gem/EF NAs. As shown in Fig. 3, the surface of SQ-gem NAs showed a supramolecular organization consisting of inverse hexagonal phases, sometimes surrounded by an amorphous layer. This 2–D organization of SQ-gem molecules could be observed directly depending on the particle arrangement with respect to the microscopy sight angle (Fig. 3A–C). This was confirmed by the geometric projection of the NAs. Such supramolecular organization has been already previously described by X-ray diffraction studies [6] but here we provide solid evidence of the particle conformation by TEM, which represents an original approach. Very importantly, this supramolecular organization was no longer observed with the multidrug SQ-gem/EF NAs, which revealed a round shape and the TEM images suggested a multilamellar onion-like structure at this resolution scale (Fig. 4A,C). In fact, Fourier transform analysis performed on SQ-gem and SQ-gem/EF NAs also detected a different periodicity, as indicated by the image spectrum analysis (Fig. 3F and 4F). The calculated mean lattice spacing between SQ-gem/ EF NAs layers was 3.6 •± 0.1 nm, instead of 3.2 •± 0.2 nm for SQ-gem NAs, which would also explain the distinct conformation and the size differences. This structural relaxation is considered to be boosted by their self-assembly mode and structure (*i.e.* lamellar instead of hexagonal). In this case and bearing in mind that the mean-lattice spacing can be independent of the number of assembled layers in terms of size, the larger distance between adjacent planes found in the SQ-gem/EF NAs was correlated with a particle shrinking.

These findings strongly support the notion that the SQ-gem/EF NAs were structurally different from the SQ-gem NAs. However, at this image resolution and given the reduced size of the NAs, it was not possible to elucidate the morphological features of SQ-gem/EF NAs thoroughly. Therefore, to go into further detail about the supramolecular organization of SQ-gem/EF NAs, the image resolution was improved by analyzing SQ-gem/EF NAs with high angle annular dark field (HAADF) high resolution scanning transmission electron microscopy (STEM). Although this imaging technique is very aggressive to organic materials due to the high voltages inflicted on the samples, image acquisitions of SQ-gem/EF NAs were obtained with a greater resolution thanks to the assistance of a negative staining agent. With this technique, we were able to confirm the multilamellar assembly of SQ-gem/EF NAs, displaying a concentric or spiral disposition of the layers (Fig. 4D,E).

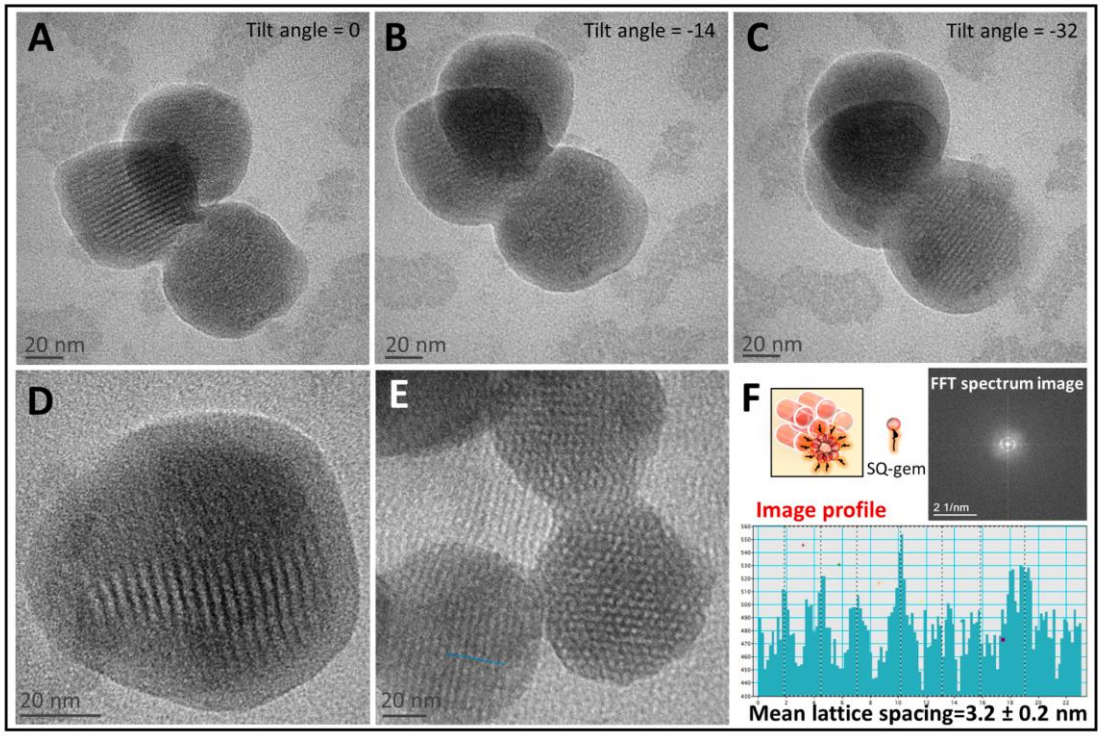

Figure 4. (A) Transmission electron microscopy images, Fourier transform image spectrum analysis and mean lattice spacing measurement of SQ-gem NAs (A) and SQ-gem/EF NAs (B). (C) High angle annular dark field (HAADF) scanning transmission electron microscopy (STEM) of SQ-gem/EF NAs (the signal corresponding to the organic material is inverted in comparison with TEM).

Thus, the incorporation of EF into SQ-gem NAs triggered drastic morphological changes. The loss of the native macromolecular structure would lead to an amorphous particle conformation, as was reported when SQ-gem was co-encapsulated with the lipophilic compound iso-combretastatin A4.[36] Nevertheless in our case Fourier transform analysis detected a periodicity, indicating that EF is co-assembled with SQ-gem due to its amphiphilic nature, which would also explain the size differences between layers. To confirm this new supramolecular organization we decided to take images of the NAs with high resolution microscopy (STEM-HAADF). Although this imaging technique is very aggressive to organic materials due to the high voltages inflicted on samples, image acquisitions of SQ-gem/EF NAs with a greater resolution were obtained with the assistance of a negative staining agent. Thus, we are able to report a multilamellar concentric organization derived from the co-assembly of the new nanosystems. This kind of structure displays physical resemblance to the onion-like multigeometry assembly of polymeric amphiphilic compounds described by Zhang *et al.*[37] and Wang *et al*.[38] In order to understand the novel particle rearrangement, we have to bear in mind that changes in the topological structures of amphiphiles can play an important role in tuning self-assembled morphologies.[39]

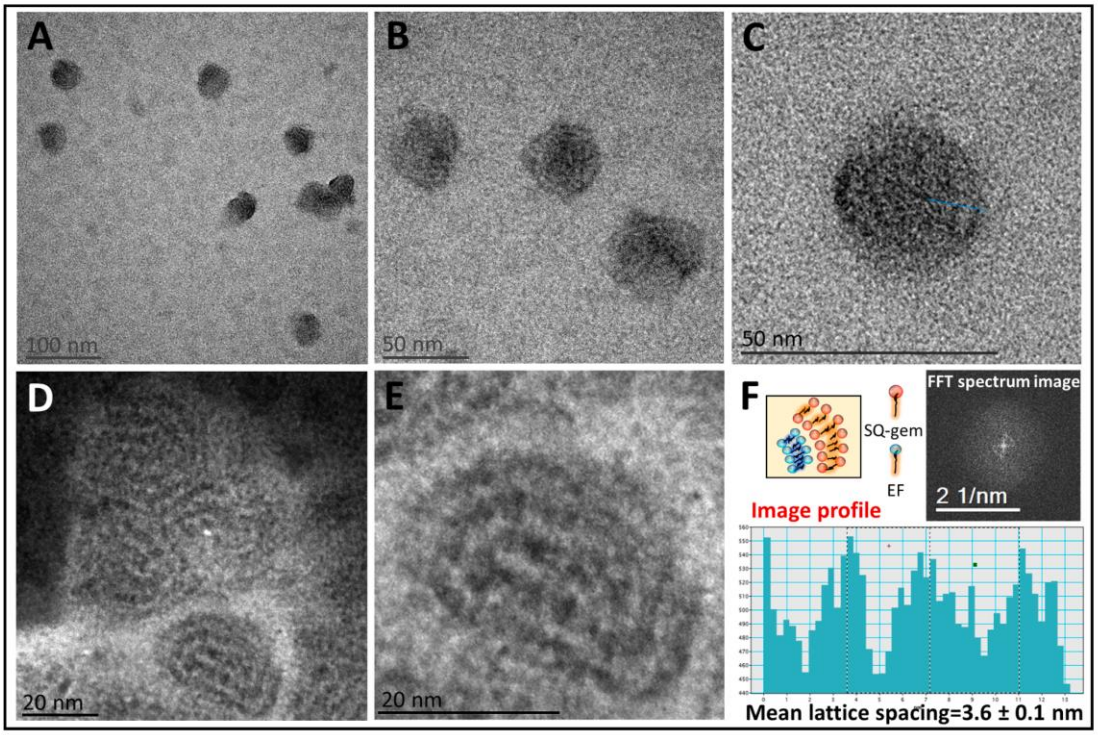

Fig. 4. Transmission electron microscopy of SQ-gem/EF NAs (A-C). High angle annular dark field (HAADF) scanning transmission electron microscopy (STEM) of SQgem/ EF NAs (D, E) (the signal corresponding to the organic material is inverted in comparison with TEM). Supramolecular organization diagram, Fourier transform image spectrum analysis and mean lattice spacing measurement of SQ-gem NAs (F).

Changes in the topological structure of amphiphilic molecules can play an important role in tuning self-assembled morphologies [38]. The loss of the native supramolecular structure of SQ-gem led to an amorphous particle conformation, as already observed when SQ-gem was coencapsulated with the lipophilic compound iso-combretastatin A4 [39]. In another study, Caron et al. formulated nanocomposites of SQ-gem monophosphate instead of SQ-gem, resulting in the formation of unilamellar vesicles [40]. Conversely, the new SQ-gem/EF NAs structure displayed physical resemblance to the onion-like multigeometry assembly of polymeric amphiphilic compounds described by Zhang et al. [41] and Wang et al. [42].

3.3. Element distribution

The distribution of elements throughout SQ-gem/EF NAs was analyzed by XPS. Survey spectra measured at the surfaces (before sputtering) of SQ-gem/EF NAs, SQ-gem NAs and free EF samples showed peaks corresponding to carbon, oxygen and nitrogen. Beside those elements, the peak belonging to the fluorine atom of Gem appeared at 687 eV. [43]. The related KLL fluorine Auger peak could also be observed (Fig. 5A). On the other hand, EF showed characteristic peaks related to the presence of phosphorus in the molecule. The presence of EF on the surface of SQ-gem/EF NAs was demonstrated by a P 2p peak clearly observed in the spectrum (Fig. 5A). The binding energy values for P 2p were 133.4 and 133.6 eV for EF and SQ-gem/EF NAs respectively. These values corresponded to the organic phosphate groups [44]. The similar binding energies found

for both samples showed an identical chemical environment, *i.e.*, there was no chemical interaction between EF phosphate groups and SQ-gem. In order to verify the presence of EF in the inner part of SQ-gem/EF NAs, depth profiling was used to study the distribution of elements throughout the particle. Since the concentration of each molecule could be related to the atomic concentration of fluorine (SQ-gem) or phosphorus (EF), the P/F atomic ratio was calculated, and its variation with etching time is shown in Fig. 5B. Etching was continued up to a point that allowed us to ensure that most of the particles had the inner part exposed. The depth profile showed that P/F atomic ratio increases from around 0.6 on the particle surface up to more than 2 after 35 s etching, corresponding to inner parts of the NAs. Thus, EF concentration was shown to be around four times the SQ-gem concentration after etching, suggesting an enrichment in this compound inside the NAs. These results indicated only a slight increase of SQ-gem concentration on the particles surface, considering that the ratio P/F was expected to be theoretically closer to 0 under equimolecular concentrations. Nevertheless, the increment of the phosphorus signal detected in a concentric multilamellar system is thought to be boosted by the higher element exposure corresponding to the inner layers. On the other hand, these results are also in agreement with UHPLC/MS/MS analysis, showing complete encapsulation of EF in the NA. A matter of concern was that EF could be only surfacting or coating the particle as a result of its phospholipid nature. Nevertheless, with XPS depth profiling analysis we were able to remove SQ-gem/EF NAs' outer layers and detect the presence of EF in inner areas. It should be borne in mind that the physico-chemical properties of SQ-gem confer an intrinsic ability to self-assemble and form stable NAs in aqueous medium, as observed in many other squalenoyl NAs [45,46]. In this sense, SQ-gem might tend to accommodate itself at the particle surface with the purpose of stabilizing the colloid dispersion, in this way displacing EF towards the inner parts.

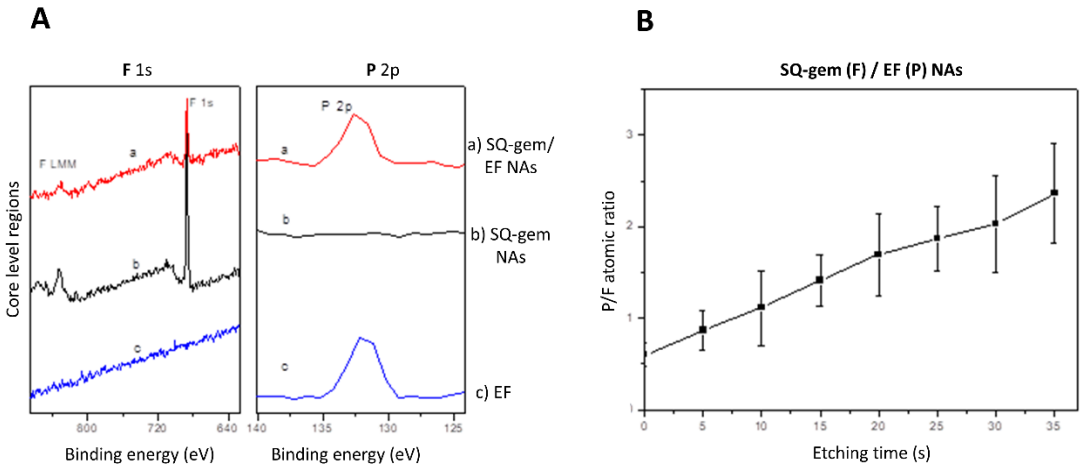

Fig. 5. Molecular tracking (X-ray photoelectron spectroscopy assays) of the fluorine (F) of SQ-gem and the phosphorus (P) of EF. (A**)** F 1s and P 2p core level regions of a) SQ-gem/EF NAs; b) SQ-gem NAs and c) free EF. (B**)** P/F atomic ratio obtained by depth profile of SQ-gem/EF NAs.

3.4. Colloid stability of SQ-gem/EF NAs

SQ-gem/EF NAs and SQ-gem NAs were analyzed for changes in the hydrodynamic diameter and PDI over 60 days. SQ-gem/EF NAs formulation was found to be stable throughout the experiment, demonstrating that the incorporation of EF did not trigger NA disruption. Indeed, as shown in Fig. 6A, no appreciable changes in the particle size were observed given that the mean particle diameter was augmented from approximately 50 up to 58 nm over two months. According to this, the PDI parameter of particle homogeneity value (Fig. 6B) only showed a slight increase and remained below the accepted values (PDI < 0.3) [47]. On the other hand, SQ-gem NAs showed colloid stability for approximately only 10 days, considering that mean particle size and PDI started to surpass desirable values at that time. These results indicated that SQ-gem/EF NAs were stable with no signs of particle disruption, agglomeration or precipitation, probably due to the presence of a complementary amphiphilic compound such as EF in the NAs. Nie et al. suggested that a regular multilamellar structure at the proper concentration ratio of components is a key factor for optimal stability [48]. The colloidal properties of the NAs were evaluated in this experiment at4 °C with regard to future administrations. This might facilitate handling and a hypothetical storage of the multidrug NAs at 2–8 °C (5 °C •± 3 °C for drug substances intended for storage in a refrigerator according to the ICH guideline Q1A(R2)). Moreover, a lyophilization process involving the incorporation of cryoprotectants or problems associated with NP reconstitution is not strictly required

.

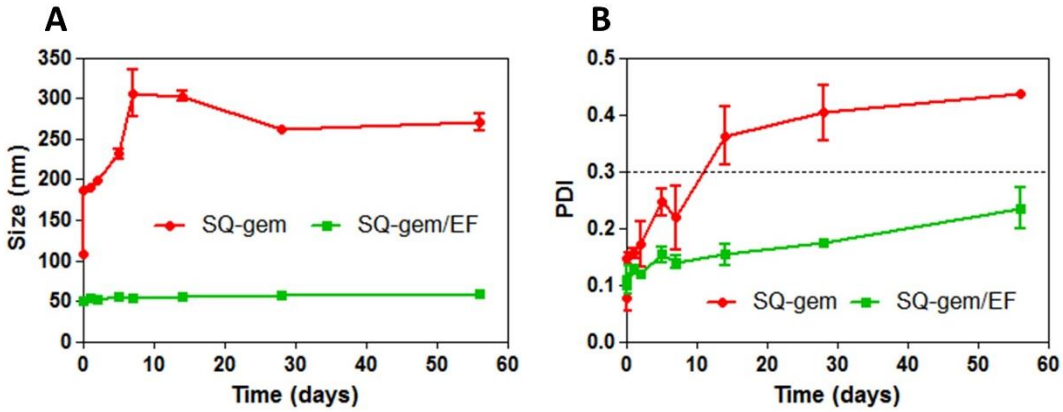

Figure 6. SQ-gem NAs (red) and SQ-gem NAs (green) stored at 4ºC are measured for particle size (A) and PDI (B) variations for 2 months.

3.5. Hemolysis activity

Hemolysis represents one of the main side effects associated with EF treatment. It is the consequence of the amphipathic structure of this compound [49], making necessary its encapsulation in drug delivery toxicity, hemolytic experiments were performed using human blood erythrocytes. *In vitro* results showed that free EF was 100% hemolytic at a concentration of 10 µg/ml, while the same concentration of EF loaded onto SQ-gem presented only 6% of hemolysis. It was concluded that SQgem/EF NAs were able to protect erythrocytes from EF associated hemolysis. The low effect produced could be

attributed to the scant presence of EF attached to the particle surface, as indicated in the XPS analysis section. An effective reduction of this toxicity represents a crucial safety aspect that determines the utility of squalenoyl nanocarriers for administering EF without compromising the patient́s health. Although SQgem/EF NAs could be also administered intraperitoneally, orally orlocally among others, it is important to consider that intravenously administered squalenoyl NAs have been reported to disassemble, being incorporated into endogenous lipoproteins [10]. However, the physicochemical features found in the SQ-gem/EF NAs suggest that they might avoid an interaction with lipoproteins, remaining longer in the circulation in their native conformation. Future experiments *in vivo* will shed light on the tumor accumulation of SQ-gem/EF NAs and as well as the hypothetical role of lipoproteins as endogenous drug delivery systems.

3.6. Anticancer activity

Cell proliferative assays revealed that these treated patient-derived cells were quite resistant to anticancer drugs due to their marked aggressive behavior. As seen in Fig. 7A, free EF showed an IC_{50} value of 69 •± 1 μM. Conversely, free Gem treatment displayed an initial higher anticancer activity but reached a plateau at 50% of cell viability, hindering IC50 calculation. SQ-gem NAs bypassed the plateau and displayed an IC50 value of 22 □} 3 μM. Importantly for our study, the insertion of EF in the NAs was not detrimental to the native antitumor activity of SQ-gem NAs. SQ-gem/EF NAs showed an IC50 value of 20 □} 2 μM for each compound (molar ratio 1:1), displaying more antitumor activity than SQ-gem NAs, especially once the threshold of 50% of cell viability was crossed (Fig. 7B). The slight IC50 improvement of the SQ-gem/EF NAs over the single SQ-gem NAs *in vitro* may be explained by the fact that part of 531M cell population remained more sensitive to Gem than to EF (Fig. 7A, first part of dark blue curve *vs* light blue curve). In this sense, the combination of free EF and free Gem at a molar ratio 1:1 also indicated that the antitumor action of EF is more visible under the threshold of 50% of cell viability. In addition, $_{SQCO2H}$/EF NAs was found to reduce the IC50 value of EF from 69 •± 1 μM to 60.5 □} 2 μM, which confirmed the suitability of the coencapsulation of EF with squalenoyl compounds. Of note, $SQCO_2H$ NAs was not observed to interfere in cell dead mechanisms given that no signs of cytotoxicity were observed below the threshold of 100 μM (Fig. 7B). The interest in using a treated patient-derived cell line as an *in vitro* model relies on the tumor resistance to conventional cytostatic agents that often leads to therapeutic failure in high-risk or relapsed patients. In this sense, we have not only provided solid evidence concerning the correct design for SQ-gem/EF NAs but also confirmed the therapeutic potential of anticancer nanomedicines. Future *in vivo* experiments that consider drug pharmacokinetics, biodistribution and NAs interaction with the primary and metastatic tumor will shed light on the real clinical profits of this new multidrug nanomedicine.

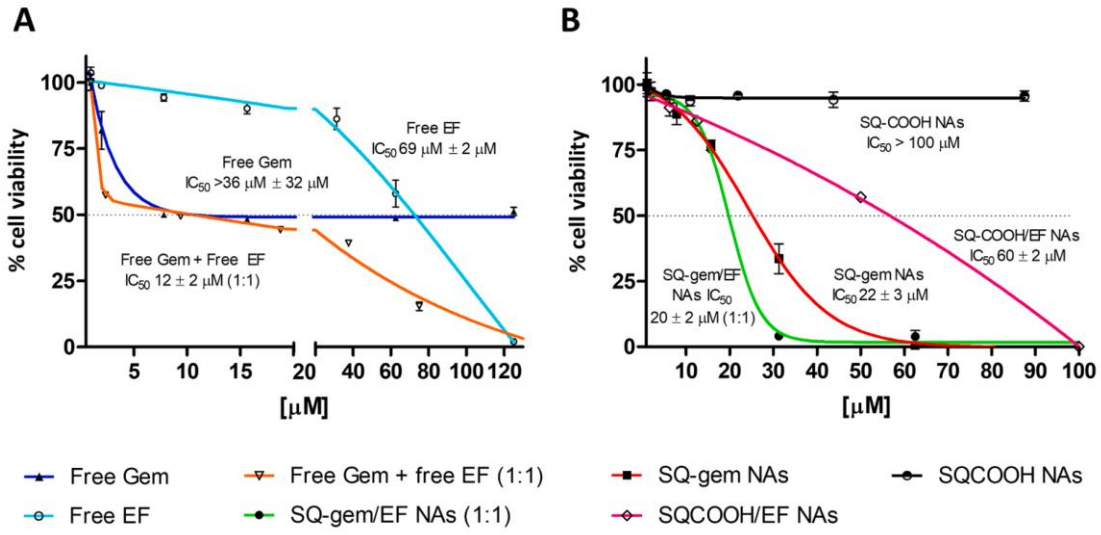

Fig. 7. Cell viability assays. 531M cells were exposed to SQ-gem/EF NAs*, SQ-gem NAs, free Gem, free EF, $SQCO_2H$/EF NAs, free Gem+free EF* and $SQCO_2H$ NAs treatments for 72 h (n ≥3, data: mean • ± SD). *X axis concentrations (μM) correspond to the individual amount of each molecule at a molar ratio 1:1.

4. CONCLUSIONS

The aim of this study was to design and characterize SQ-gem/EF NAs usable as multitherapy nanodevices in cancer therapy. The results of this study show that the alkyl-lysophospholipid EF was able to coassemble with the pro-drug SQ-gem to form NAs with no need to use any stabilizer. We provide insights into an easy formulation process for this nanomedicine with drugs only by leveraging their amphiphilic nature. At a molecular ratio of 1:1, NAs displayed reproducible and homogeneous formulation batches of 51 • } 1 nm. This is a considerable particle size reduction over SQ-gem NAs, and also provides a substantial increment in the drug content, up to 67.28 wt%. This co-assembly led to a new supramolecular arrangement, showing a multilamellar concentric conformation. SQ-gem NAs have previously shown great anticancer activity in various tumor models. An important fact that reinforces the combination with EF is that it acts not only as a second antitumor agent but also as a NP stabilizer. *In vitro*, the SQ-gem/ EF NAs suppressed the hemolytic activity of EF, a major side effect of this molecule, and presented a better antitumor profile than SQ-gem NAs.

In this work we have designed and formulated a novel multidrug nanomedicine. Its biocompatible nature and high drug content make it a suitable pre-clinical candidate for cancer therapy.

Acknowledgements

Asociacion Espanola Contra el Cancer (AECC) (CI14142069BLAN) (Spain) and Fundacion Caja Navarra/Obra Social La Caixa are gratefully acknowledged. CIBER-BBN is an initiative funded by theVI Spanish National R&D&i Plan 2008–2011 , Iniciativa Ingenio 2010, Consolider Program, CIBER Actions (Spain) and financed by the Instituto de Salud Carlos III (Spain) with assistance from the European Regional Development Fund.

Declaration of Competing Interest

The authors declare no competing interests.

REFERENCES

(1) Hassan, S.; Prakash, G.; Bal Ozturk, A.; Saghazadeh, S.; Farhan Sohail, M.; Seo, J.; Remzi Dokmeci, M.; Zhang, Y. S.; Khademhosseini, A. Evolution and Clinical Translation of Drug Delivery Nanomaterials. *Nano Today* **2017**, *15*, 91–106.

(2) Peer, D.; Karp, J. M.; Hong, S.; Farokhzad, O. C.; Margalit, R.; Langer, R. Nanocarriers as an Emerging Platform for Cancer Therapy. *Nat. Nanotechnol.* **2007**, *2* (12), 751–760.

(3) Shi, J.; Kantoff, P. W.; Wooster, R.; Farokhzad, O. C. Cancer Nanomedicine: Progress, Challenges and Opportunities. *Nat. Rev. Cancer* **2016**, *17* (1), 20–37.

(4) Hartshorn, C. M.; Bradbury, M. S.; Lanza, G. M.; Nel, A. E.; Rao, J.; Wang, A. Z.; Wiesner, U. B.; Yang, L.; Grodzinski, P. Nanotechnology Strategies To Advance Outcomes in Clinical Cancer Care. *ACS Nano* **2018**, *12* (1), 24–43.

(5) Lu, Z.-R.; Qiao, P. Drug Delivery in Cancer Therapy, Quo Vadis? *Mol. Pharm.* **2018**, DOI: 10.1021/acs.molpharmaceut.8b00037.

(6) Couvreur, P.; Reddy, L. H.; Mangenot, S.; Poupaert, J. H.; Desmaële, D.; Lepêtre-Mouelhi, S.; Pili, B.; Bourgaux, C.; Amenitsch, H.; Ollivon, M. Discovery of New Hexagonal Supramolecular Nanostructures Formed by Squalenoylation of an Anticancer Nucleoside Analogue. *Small* **2008**, *4* (2), 247–253.

(7) Arias, J. L.; Reddy, L. H.; Othman, M.; Gillet, B.; Desmaële, D.; Zouhiri, F.; Dosio, F.; Gref, R.; Couvreur, P. Squalene Based Nanocomposites: A New Platform for the Design of Multifunctional Pharmaceutical Theragnostics. *ACS Nano* **2011**, *5* (2), 1513–1521.

(8) Gaudin, A.; Yemisci, M.; Eroglu, H.; Lepetre-Mouelhi, S.; Turkoglu, O. F.; Dönmez-Demir, B.; Caban, S.; Sargon, M. F.; Garcia-Argote, S.; Pieters, G.; *et al.* Squalenoyl Adenosine Nanoparticles Provide Neuroprotection after Stroke and Spinal Cord Injury. *Nat. Nanotechnol.* **2014**, *9* (12), 1054–1062.

(9) Couvreur, P.; Stella, B.; Reddy, L. H.; Hillaireau, H.; Dubernet, C.; Desmaële, D.; Lepêtre-Mouelhi, S.; Rocco, F.; Dereuddre-Bosquet, N.; Clayette, P.; *et al.* Squalenoyl Nanomedicines as Potential Therapeutics. *Nano Lett.* **2006**, *6* (11), 2544–2548.

(10) Sobot, D.; Mura, S.; Yesylevskyy, S. O.; Dalbin, L.; Cayre, F.; Bort, G.; Mougin, J.; Desmaële, D.; Lepetre-Mouelhi, S.; Pieters, G.; et al. Conjugation of Squalene to Gemcitabine as Unique Approach Exploiting Endogenous Lipoproteins for Drug Delivery. *Nat. Commun.* **2017**, *8*, 15678.

(11) Réjiba, S.; Reddy, L. H.; Bigand, C.; Parmentier, C.; Couvreur, P.; Hajri, A. Squalenoyl Gemcitabine Nanomedicine Overcomes the Low Efficacy of Gemcitabine Therapy in Pancreatic Cancer. *Nanomedicine Nanotechnology, Biol. Med.* **2011**, *7* (6), 841–849.

(12) Gaudin, A.; Song, E.; King, A. R.; Saucier-Sawyer, J. K.; Bindra, R.; Desmaële,

D.; Couvreur, P.; Saltzman, W. M. PEGylated Squalenoyl-Gemcitabine Nanoparticles for the Treatment of Glioblastoma. *Biomaterials* **2016**, *105*, 136–144.

(13) Ward, S.; Morris, E.; Bansback, N.; Calvert, N.; Crellin, A.; Forman, D.; Larvin, M.; Radstone, D. A Rapid and Systematic Review of the Clinical Effectiveness and Cost-Effectiveness of Gemcitabine for the Treatment of Pancreatic Cancer. *Health Technol. Assess.* **2001**, *5* (24), 1–70.

(14) Sandler, A.; Ettinger, D. S. Gemcitabine: Single-Agent and Combination Therapy in Non-Small Cell Lung Cancer. *Oncologist* **1999**, *4* (3), 241–251.

(15) Ciccolini, J.; Serdjebi, C.; Peters, G. J.; Giovannetti, E. Pharmacokinetics and Pharmacogenetics of Gemcitabine as a Mainstay in Adult and Pediatric Oncology: An EORTC-PAMM Perspective. *Cancer Chemother. Pharmacol.* **2016**, *78* (1), 1–12.

(16) Gaudin, A.; Lepetre-Mouelhi, S.; Mougin, J.; Parrod, M.; Pieters, G.; Garcia-Argote, S.; Loreau, O.; Goncalves, J.; Chacun, H.; Courbebaisse, Y.; *et al.* Pharmacokinetics, Biodistribution and Metabolism of Squalenoyl Adenosine Nanoparticles in Mice Using Dual Radio-Labeling and Radio-HPLC Analysis. *J. Control. Release* **2015**, *212*, 50–58.

(17) Reddy, L. H.; Marque, P.-E.; Dubernet, C.; Mouelhi, S.-L.; Desmaele, D.; Couvreur, P. Preclinical Toxicology (Subacute and Acute) and Efficacy of a New Squalenoyl Gemcitabine Anticancer Nanomedicine. *J. Pharmacol. Exp. Ther.* **2008**, *325* (2), 484–490.

(18) Hu, C.-M. J.; Aryal, S.; Zhang, L. Nanoparticle-Assisted Combination Therapies for Effective Cancer Treatment. *Ther. Deliv.* **2010**, *1* (2), 323–334.

(19) Ma, W.; Cheetham, A. G.; Cui, H. Building Nanostructures with Drugs. *Nano Today* **2016**, *11* (1), 13–30.

(20) González-Fernández, Y.; Imbuluzqueta, E.; Zalacain, M.; Mollinedo, F.; Patiño-García, A.; Blanco-Prieto, M. J. Doxorubicin and Edelfosine Lipid Nanoparticles Are Effective Acting Synergistically against Drug-Resistant Osteosarcoma Cancer Cells. *Cancer Lett.* **2017**, *388*, 262–268.

(21) Estella-Hermoso de Mendoza, A.; Préat, V.; Mollinedo, F.; Blanco-Prieto, M. J. *In Vitro* and *in Vivo* Efficacy of Edelfosine-Loaded Lipid Nanoparticles against Glioma. *J. Control. Release* **2011**, *156* (3), 421–426.

(22) Aznar, M. Á.; Lasa-Saracíbar, B.; Estella-Hermoso de Mendoza, A.; Blanco-Prieto, M. J. Efficacy of Edelfosine Lipid Nanoparticles in Breast Cancer Cells. *Int. J. Pharm.* **2013**, *454* (2), 720–726.

(23) Castro, B. M.; Fedorov, A.; Hornillos, V.; Delgado, J.; Acuña, A. U.; Mollinedo, F.; Prieto, M. Edelfosine and Miltefosine Effects on Lipid Raft Properties: Membrane Biophysics in Cell Death by Antitumor Lipids. *J. Phys. Chem. B* **2013**, *117* (26), 7929–7940.

(24) P. Rios-Marco, C. Marco, X. Galvez, J.M. Jimenez-Lopez, M.P. Carrasco, Alkylphospholipids: an update on molecular mechanisms and clinical relevance, Biochim. Biophys. Acta. 1859 (2017) 1657–1667.

(25) Lasa-Saracíbar, B.; Aznar, M. Á.; Lana, H.; Aizpún, I.; Gil, A. G.; Blanco-Prieto, M. J. Lipid Nanoparticles Protect from Edelfosine Toxicity *in Vivo*. *Int. J. Pharm.* **2014**, *474* (1–2), 1–5.

(26) Estella-Hermoso de Mendoza, A.; Campanero, M. A.; Lana, H.; Villa-Pulgarin, J. A.; de la Iglesia-Vicente, J.; Mollinedo, F.; Blanco-Prieto, M. J. Complete Inhibition of Extranodal Dissemination of Lymphoma by Edelfosine-Loaded Lipid Nanoparticles. *Nanomedicine* **2012**, *7* (5), 679–690.

(27) Estella-Hermoso de Mendoza, A.; Campanero, M. A.; Mollinedo, F.; Blanco-Príeto, M. J. Comparative Study of A HPLC–MS Assay versus an UHPLC–MS/MS for Anti-Tumoral Alkyl Lysophospholipid Edelfosine Determination in Both Biological Samples and in Lipid Nanoparticulate Systems. *J. Chromatogr. B* **2009**, *877* (31), 4035–4041.

(28) Khoury, H.; Deroussent, A.; Reddy, L. H.; Couvreur, P.; Vassal, G.; Paci, A. Simultaneous Determination of Gemcitabine and Gemcitabine-Squalene by Liquid Chromatography-Tandem Mass Spectrometry in Human Plasma. *J. Chromatogr. B. Analyt. Technol. Biomed. Life Sci.* **2007**, *858* (1–2), 71–78.

(29) Reddy, L. H.; Renoir, J.-M.; Marsaud, V.; Lepetre-Mouelhi, S.; Desmaële, D.; Couvreur, P. Anticancer Efficacy of Squalenoyl Gemcitabine Nanomedicine on 60 Human Tumor Cell Panel and on Experimental Tumor. *Mol. Pharm.* **2009**, *6* (5), 1526–1535.

(30) Busto, J. V.; Sot, J.; Goñi, F. M.; Mollinedo, F.; Alonso, A. Surface-Active Properties of the Antitumour Ether Lipid 1-O-Octadecyl-2-O-Methyl-Rac-Glycero-3-Phosphocholine (Edelfosine). *Biochim. Biophys. Acta - Biomembr.* **2007**, *1768* (7), 1855–1860.

(31) C. Bastiancich, K. Vanvarenberg, B. Ucakar, M. Pitorre, G. Bastiat, F. Lagarce, V. Preat, F. Danhier, Lauroyl-gemcitabine-loaded lipid nanocapsule hydrogel for the treatment of glioblastoma, J. Control. Release 225 (2016) 283–293.

(32) Karmali, P. P.; Simberg, D. Interactions of Nanoparticles with Plasma Proteins: Implication on Clearance and Toxicity of Drug Delivery Systems. *Expert Opin. Drug Deliv.* **2011**, *8* (3), 343–357.

(33) Rosenblum, D.; Joshi, N.; Tao, W.; Karp, J. M.; Peer, D. Progress and Challenges towards Targeted Delivery of Cancer Therapeutics. *Nat. Commun.* **2018**, *9* (1), 1410.

(37) Savla, R.; Minko, T. Nanoparticle Design Considerations for Molecular Imaging of Apoptosis: Diagnostic, Prognostic, and Therapeutic Value. *Adv. Drug Deliv. Rev.* **2017**, *113*, 122–140.

(35) Bertrand, N.; Wu, J.; Xu, X.; Kamaly, N.; Farokhzad, O. C. Cancer Nanotechnology: The Impact of Passive and Active Targeting in the Era of Modern Cancer Biology. *Adv. Drug Deliv. Rev.* **2014**, *66*, 2–25.

(36) Cabral, H.; Matsumoto, Y.; Mizuno, K.; Chen, Q.; Murakami, M.; Kimura, M.; Terada, Y.; Kano, M. R.; Miyazono, K.; Uesaka, M.; et al. Accumulation of Sub-100 Nm Polymeric Micelles in Poorly Permeable Tumours Depends on Size. *Nat. Nanotechnol.* **2011**, *6* (12), 815–823.

(37) Karageorgis, A.; Dufort, S.; Sancey, L.; Henry, M.; Hirsjärvi, S.; Passirani, C.; Benoit, J.-P.; Gravier, J.; Texier, I.; Montigon, O.; *et al.* An MRI-Based Classification Scheme to Predict Passive Access of 5 to 50-Nm Large Nanoparticles to Tumors. *Sci. Rep.* **2016**, *6* (1), 21417.

(38) Wang, Z.; Wang, H.; Cheng, M.; Li, C.; Faller, R.; Sun, S.; Hu, S. Controllable Multigeometry Nanoparticles *via* Cooperative Assembly of Amphiphilic Diblock Copolymer Blends with Asymmetric Architectures. *ACS Nano* **2018**, 12, 1413−1419.

(39) Maksimenko, A.; Alami, M.; Zouhiri, F.; Brion, J.-D.; Pruvost, A.; Mougin, J.; Hamze, A.; Boissenot, T.; Provot, O.; Desmaële, D.; *et al.* Therapeutic Modalities of Squalenoyl Nanocomposites in Colon Cancer: An Ongoing Search for Improved Efficacy. *ACS Nano* **2014**, *8* (3), 2018–2032.

(40) J. Caron, E. Lepeltier, L.H. Reddy, S. Lepetre-Mouelhi, S. Wack, C. Bourgaux, P. Couvreur, D. Desmaele, Squalenoyl gemcitabine monophosphate: synthesis, characterisation of nanoassemblies and biological evaluation, European J. Org. Chem. 2011 (2011) 2615–2628.

(41) Zhang, K.; Gao, L.; Chen, Y.; Yang, Z. Onion-like Microspheres with Tricomponent from Gelable Triblock Copolymers. *J. Colloid Interface Sci.* **2010**, *346* (1), 48–53.

(42) Wang, J.; Wang, X.; Yang, F.; Shen, H.; You, Y.; Wu, D. Effect of Topological Structures on the Self-Assembly Behavior of Supramolecular Amphiphiles. *Langmuir* **2015**, *31* (51), 13834–13841.

(43) Parsian, M.; Unsoy, G.; Mutlu, P.; Yalcin, S.; Tezcaner, A.; Gunduz, U. Loading of Gemcitabine on Chitosan Magnetic Nanoparticles Increases the Anti-Cancer Efficacy of the Drug. *Eur. J. Pharmacol.* **2016**, *784*, 121–128.

(44) K.S. Siow, L. Britcher, S. Kumar, H.J. Griesser, Deposition and XPS and FTIR analysis of plasma polymer coatings containing phosphorus, plasma process, Polym. 11 (2014) 133–141.

(45) Maksimenko, A.; Dosio, F.; Mougin, J.; Ferrero, A.; Wack, S.; Reddy, L. H.; Weyn, A.-A.; Lepeltier, E.; Bourgaux, C.; Stella, B.; et al. A Unique Squalenoylated and Nonpegylated Doxorubicin Nanomedicine with Systemic Long-Circulating Properties and Anticancer Activity. *Proc. Natl. Acad. Sci.* **2014**, *111* (2), E217–E226.

(46) Dosio, F.; Reddy, L. H.; Ferrero, A.; Stella, B.; Cattel, L.; Couvreur, P. Novel Nanoassemblies Composed of Squalenoyl−Paclitaxel Derivatives: Synthesis, Characterization, and Biological Evaluation. *Bioconjug. Chem.* **2010**, *21* (7), 1349–1361.

(47) Danaei, M.; Dehghankhold, M.; Ataei, S.; Hasanzadeh Davarani, F.; Javanmard, R.; Dokhani, A.; Khorasani, S.; Mozafari, M. Impact of Particle Size and Polydispersity Index on the Clinical Applications of Lipidic Nanocarrier Systems. *Pharmaceutics* **2018**, *10* (2), 57.

(47) M. Danaei, M. Dehghankhold, S. Ataei, F. Hasanzadeh Davarani, R. Javanmard, A. Dokhani, S. Khorasani, M. Mozafari, Impact of particle size and

polydispersityindex on the clinical applications of lipidic nanocarrier systems, *Pharmaceutics* 10 (2018) 57.

(48) S. Nie, X. Zhang, R. Gref, P. Couvreur, Y. Qian, L. Zhang, Multilamellar nanoparticles self-assembled from opposite charged blends: insights from mesoscopic simulation, *J. Phys. Chem. C* 119 (2015) 20649–20661.

(49) J. Kotting, N.W. Marschner, W. Neumuller, C. Unger, H. Eibl, Hexadecylphosphocholine and octadecyl-methyl-glycero-3-phosphocholine: acomparison of hemolytic activity, serum binding and tissue distribution, Prog. Exp. Tumor Res. 34 (1992) 131–142.

ACKNOWLEDGEMENTS

Asociación Española Contra el Cáncer (AECC) (CI14142069BLAN) and Fundación Caja Navarra/Obra Social La Caixa are gratefully acknowledged. CIBER-BBN is an initiative funded by the VI Spanish National R&D&i Plan 2008–2011, Iniciativa Ingenio 2010, Consolider Program, CIBER Actions and financed by the Instituto de Salud Carlos III (Spain) with assistance from the European Regional Development Fund.

Competing interests statement

The authors declare no competing interests.